KSCE Journal of Civil Engineering (2018) 22(2):494-508
DOI 10.1007/s12205-017-0841-1

Geotechnical Engineering
pISSN 1226-7988, eISSN 1976-3808
www.springer.com/12205

Optimised Design of Jet-grouted Rafts Subjected to Nonuniform Vertical Loading

Halil Murat Algin*

Received October 10, 2015/Accepted March 18, 2017/Published Online May 19, 2017

Abstract

A parametric study based on three dimensional finite element (3D FE) simulations of jet-grouted rafts (JGRs) subjected to nonuniform vertical loading has been conducted to investigate the interactions of JGR elements that are raft, jet-grouted columns (JGCs), granular interlayer mat and subsoil. The presented initial 3D FE simulation of a single JGC which is geometrically approximated with the rotated sinusoidal functional representation accounting for the actual variation of JGC diameter with depth is validated performing the back-analysis of the developed 3D FE models with the well-known experimental results reported in the literature. The image processing technique allowing the 3D FE modelling of complex irregular geometries has been employed and the extension of simulation to the complete JGR system is accomplished. Considering the design strategies previously defined for JGR systems, Paper resolves how the independent variables of interlayer thickness, JGC spacing and length under the core and edge areas of raft affect the design responses of settlements, bending moments and vertical stresses. The multi objective optimization analysis has been performed using Response Surface Method (RSM) to achieve the most economical design solution that satisfies the presented design constraints for JGRs. The effects of design constraints on the optimised design are presented graphically. Paper concludes the coupling of design strategies defined separately for JGC and piled raft provides opportunity to achieve the optimised design of complete JGR systems using 3D FE simulation with the image processing technique and RSM.

Keywords: *Jet grouting, jet-grouted raft, foundation design, finite element analysis, optimization*

1. Introduction

Jet grouting has become very popular worldwide as a practical technique to solve several geotechnical problems. The high-pressure injection of a grout (generally water-cement mixture) within previously drilled small boreholes breaks up the surrounding soil and mixes it with a self-hardening grout (Yahiro and Yoshida, 1973). Since it provides a quasi-cylindrical shaped columns of cemented soil (soilcrete), this process allows to construct columns, panels or other structures in the ground with limited disturbance of the surrounding soil. This technique can be alternative to piles for the economic reasons if there are large rock masses interspersed in the soil matrix (Croce *et al*., 2014). In the case of using Jet-grouted Columns (JGCs) as a raft supporting system with centre-to-centre spacing, this arrangement named as Jet-grouted Raft (JGR) becomes similar to the piled raft design (Croce *et al*., 2014). JGCs are generally used as settlement reducers rather than for ensuring the overall stability of the foundation. If necessary, JGCs are reinforced by inserting steel tubes, bars or other reinforcing elements to increase the tensile and flexural strength of JGCs or inclined to take up the additional horizontal load component (Falcao *et al*., 2001). The cushion is a granular interlayer mat placed between the raft and the soil to reduce the stress concentration. Considering the effects of JGCs the concept of JGR design differs from the traditional raft design (Algin, 2016).

Regarding the design of JGCs, the current rules, codes of practice and guidelines are not homogenous around the world. The standards in Germany and Italy (AGI, 2012; DIN-4093, 2012) issue specific rules on the design of jet grouting by suggesting the design path to be organised and provide the quantitative indications on some important design parameters. The national guidelines in Japan (JJGA, 2005) however provides the encompass indications on design and a strong deterministic approach, even the geometrical choices (grid, array and spacing) are constrained and taken out of the responsibility of the designer (Croce *et al*., 2014). The European standards (BS-EN-12716, 2001) and U.S. guidelines (GI-ASCE, 2009) provide a sequential list of activities should be followed in a typical jet grouting project and highlight the role of preliminary field trials and the quality control-assurance tests for quantifying the jet grouting properties.

The previous studies show that the values of diameters and unconfined compressive strength of JGCs vary depending on the original soil properties and the combination of injection systems (e.g., (Croce *et al.*, 2001; Flora *et al.*, 2013; Modoni *et al*., 2006; Xanthakos *et al.*, 1994)). The heterogeneity of subsoil provides dominant effect on the local variation of diameters and strength of JGCs that affects the overall JGC resistance (Croce *et al.*, 2001; Croce and Modoni, 2002). In order to analyse the complete

*Professor, Harran University, Civil Engineering Dept., Osmanbey Campus 63000, Şanlıurfa, Turkey (Corresponding Author, E-mail: hmalgin@harran.edu.tr)

JGR system, it is important to quantify the interaction between JGCs and the surrounding soil to identify how lateral interface stresses and end-bearing loads are mobilised with settlements and correlated with the geometry of JGCs. This mechanism has been investigated by several authors (Bustamante, 2002; Bzówka, 2009; Cicognani and Garassino, 1989; Garassino, 1997; Maertens and Maekelberg, 2001) using full-scale experiments and they generally agree that high loads are transferred to the surrounding soil from the lateral surface of JGCs.

The optimum design strategies of piled rafts investigated by several authors indicate that bending moment, maximum and differential settlements of raft are important design parameters (e.g., (Leung *et al.*, 2010; Nakanishi and Takewaki, 2013; Reul and Randolph, 2004)). Along these dependent variables, the design parameters of JGC that are lateral interface stresses, end-bearing loads and axial column stresses are demonstrated to be important parameters for the JGR design (Algin, 2016). The limits of these constraining parameters defined previously for pilled raft (Reul and Randolph, 2004) and JGC design responses (Croce *et al.,* 2014) are coupled in this paper for the optimised design analysis of JGR subjected to nonuniform loading.

Response Surface Method (RSM) that is used in the presented multi-objective optimization analysis provides comprehensive solution for the overall response system and has recently been applied to the JGR design by Algin (2016). Variance analysis is performed prior to the design optimisation to ensure that the dependent variables are significantly related to the considered independent variables that are cushion thickness, the column spacing and the column length varies under the core and edge areas of the raft.

In this paper, the rotated sinusoidal function was used for the approximation of complex irregular shapes of JGCs and compared with the prediction developed by Modoni *et al.* (2006). Paper demonstrates that since the rotated sinusoidal function is a harmonic function, this functional prediction can be used as a geometrical representation for JGCs. The different field trial data (Vesuvius (Croce and Flora, 1998), Polcevera (Croce *et al.*, 1994) and Barcelona (Arroyo *et al.*, 2007)) previously presented by Modoni and Bzowka (2012) are used in this paper to demonstrate that the presented functional prediction is adequately approximate the geometrical variation of JGCs.

The image processing technique allowing the modelling of complex irregular geometries has been employed in this study for three dimensional finite element (3D FE) modelling of system elements. This robust technique enabled the 3D FE modelling of this complex geometrical shape of JGCs. The parameter for the JGC-soil interface is obtained and validated by performing the back-analysis of the developed 3D FE models with the well-known experimental results reported in the literature (Modoni and Bzowka, 2012). The presented soil profile and its related parameters (Modoni and Bzowka, 2012) are adopted in the presented FE modelling.

The aim of this paper is to demonstrate how the realistic JGC geometries represented by the rotated sinusoidal function can accurately be modelled in the 3D FE simulations using the image processing technique, how the JGR optimum design strategies can be adopted on this functional prediction of columns, how the design limitations affect the optimized design solution and how the nonuniform vertical loading applied on the JGR system influences the considered design variables that are cushion thickness, the column spacing and the column length varies under the core and edge areas of the raft.

2. 3D FE Simulation of a Single Column Geometrically Represented with the Rotated Sinusoidal Function

The previous studies on JGCs summarised by Croce *et al.*

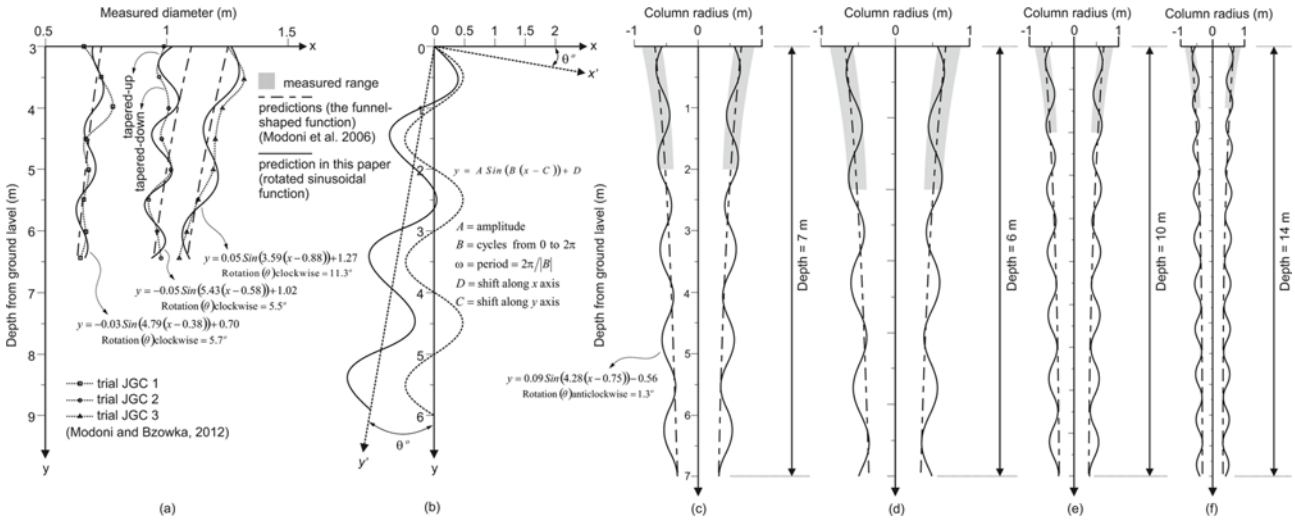

Fig. 1. Geometrical Representation of JGCs: (a) the Rotated Sinusoidal Functions Adopted to the Measured Diameters with Depth for Three Trial JGCs, (b) the General Definitions of Rotated Sinusoidal Function; the Rotated Sinusoidal Function Adopted to the Measured Diameter Range of Trial JGC Having, (c) 7 m Height, (d) 6 m Height, (e) 10 m Height and (f) 14 m Height

Table 1. Mean Square Error (MSE) and Mean Absolute Relative Error (MARE) Values to Compare the Theoretical Funnel-shaped Functional Prediction and the Geometrical Representation of Measured Data with the Rotated Sinusoidal Function

	Assumption of the rotated sinusoidal function		Assumption of the funnel-shaped function*, **	
	Mean Square Error (m^2)	Mean Absolute Relative Error (%)	Mean Square Error (m^2)	Mean Absolute Relative Error (%)
Trial column 1**	0.0007	3.1505	0.0014	4.1572
Trial column 2**	0.0007	2.5225	0.0038	5.1738
Trial column 3**	0.0011	2.6708	0.002	2.7938

*) Modoni *et al.* (2006), **) Modoni and Bzowka (2012)

(2014) have clearly demonstrated that the soil properties influence the column diameters and the treatment procedure to be introduced. In order to predict the column diameter, some empirical correlations (e.g., (AGI, 2012; Bell, 1993; Botto, 1985; Flora and Lirer, 2011; Flora *et al.*, 2013; Kutzner, 1996; Lesnik, 2001; Tornaghi and Pettinaroli, 2004; Xanthakos *et al.*, 1994)) and the theoretical models (e.g., (Chu, 2005; Heng, 2008; Modoni *et al.*, 2006; Wang *et al.*, 2012)) are generally used and the most of these researches agree that if the friction angle of soil is of higher value, the diameter variation of a single column progressively reduces with depth due to the increase in the effective stress (Croce *et al.*, 2014; Modoni and Bzowka, 2012). There is more or less a reducing trend with depth if a comparison is made between the top and button diameter of JGC. Because of the uncertainties involved in the prediction of the column properties and the diameter variation, the field trials are recommended for the application of JGCs (e.g. (BS-EN-12716, 2001; GI-ASCE, 2009)).

Figure 1(a) shows the measured diameters with depth for three trial JGCs (Vesuvius (Croce and Flora, 1998), Polcevera (Croce *et al.*, 1994) and Barcelona (Arroyo *et al.*, 2007)) (Modoni and Bzowka, 2012) constructed in the similar soil type with different jet energies clearly demonstrate this reduction trend in JGCs. This trend can be predicted by empirical (e.g., (Kutzner, 1996)) or theoretical (e.g. (Modoni *et al.*, 2006)) relations which should be considered only as a mean dimensional variation because the local probable discrepancies might occur due to the sudden variations in soil properties (Miki and Nakanishi, 1984). Modoni and Bzowka (2012) presented the functional prediction to these trial JGCs shown in Fig. 1(a). Although, this prediction is based on a distinguished theoretical background on the basis of the theory of submerged flow and the seepage model for jet–soil interaction, as stated by the authors (Modoni and Bzowka, 2012) it only demonstrates the average dimensional variations disregarding the local conversions. It was previously demonstrated for the traditional piles that the geometrical variation with depth significantly influence the resulting stresses in piles and soil (Shahu, 2006). Such a geometrical variation is demonstrated for the trial JGC 2 in Fig. 1(a). The tapered-up section is observed between the depths of 3 m and 3.5 m, and then the tapered-down section is followed between the depths of 3.5 m and 4 m (Fig. 1(a)). Since these tapered-up and down geometrical variations of JGCs significantly influence the resulting stress values and continuously observed with the column depth (Fig. 1(a)), the rotated sinusoidal function shown in Fig. 1(b) is used for the modelling of JGCs and it only demonstrates the geometrical shape representation of JGCs. The *sine* function is a harmonic function, it can easily be adjusted to the measured data using its numerical values (*A*, *B*, *C* and *D* shown in Figs. 1(a) and 1(b)). The additional rotation of *sine* function yields the general trend of the diameter reduction in depth (Fig. 1(a)). Mean Square Error (MSE) and Mean Absolute Relative Error (MARE) values are calculated to compare the funnel-shaped and the rotated sinusoidal functions using the measured data given in each 0.5 m depth (Table 1 and Fig. 1(a)). Apart from better representation capability of the rotated sinusoidal function following the tapered-up and down sections (Fig. 1(a)), unlike the funnel-shaped functional prediction Table 1 shows that the *sine* functions (Fig. 1(a)) represents the measured data more closely considering the local diameter variations in JGC geometries.

The well-known experimental study on four JGCs carried out in the municipality of Bojszowy Nowe, Poland was reported by Bzówka (2009) and Bzówka and Pieczyrak (2008). The axial loading test on the column having the length of 7.0 m has been the bases of the FE simulation presented by Modoni and Bzowka (2012). It was reported (Modoni and Bzowka, 2012) that the rest of the columns were reinforced with HEB 240 steel bars and the variation of diameter was only measured in the top 2 m above the water table as illustrated with the shaded area in Fig. 1(c). The theoretical function developed by Modoni *et al.* (2006) was presented with the dashed line in Fig. 1(c) (Modoni and Bzowka, 2012). As demonstrated in Fig. 1(c) the rotated sinusoidal function is in a good agreement with both the theoretical funnel-shaped functional prediction and the measured data range. This harmonic function is also used for the JGCs having the length of 6 m, 10 m and 14 m shown in Figs. 1(d)-1(f).

Several piezocone (CPTU) and flat dilatometer (DMT) tests were performed near JGCs in the study of Bojszowy Nowe field trials (Bzówka, 2009; Bzówka and Pieczyrak, 2008; Modoni and Bzowka, 2012) to identify the composition and the stress-strain properties of the soil. Fig. 2 summarizes the obtained soil profile that is used for the FE soil modelling by Modoni and Bzowka (2012). The nine overlapped soil layers shown in Fig. 2(c) are defined in the soil profile to simplify the complexity of modelling presented in this paper and the corresponding averaged geotechnical parameters are demonstrated in Figs. 2(a) and 2(b). As illustrated in Fig. 2(c) each subsoil layer is assigned to an individual grayscale value used for the image processing to create the

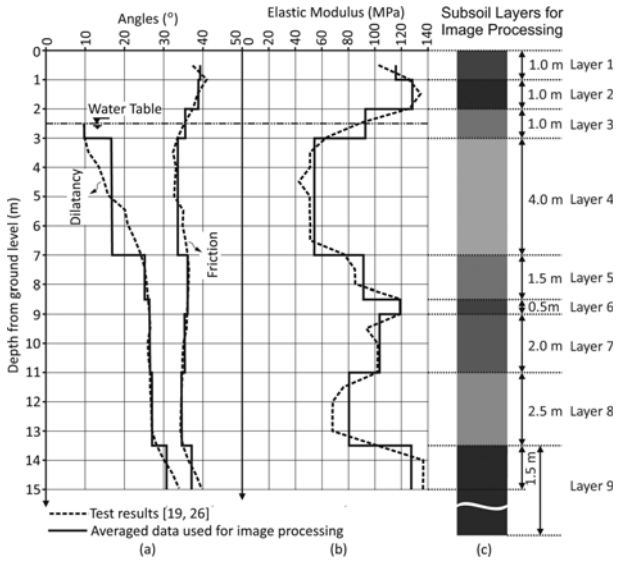

Fig. 2. The Soil Profile Used for 3D FE Soil Modelling: (a) the Friction and Dilatancy Angles, (b) the Elastic Modulus, (c) the Sub-layering of Soil with Grayscaling Used in the Image Processing

filtered volumetric 3D data following the method presented previously (Algin, 2016). Fig. 3 illustrates these image processing stages undertaken. Accordingly, the soil volume is then transferred into Abaqus (2012) as a CAD model for the 3D mesh generation presented in Fig. 4. The rotated sinusoidal function given in Fig. 1(c) is used for the 3D FE modelling of Bojszowy Nowe field trial having 7 m column length without the steel reinforcement on which the axial loading test has been undertaken. The quarter of the model shown in Fig. 4 has been analysed for the simplicity. As to boundary conditions, the bottom surface is vertically supported, and the roller constraint is assigned to all of the external vertical surfaces. The constitutive parameters adopted from Modoni and Bzowka (2012)f or the FE model are presented in Table 2 and Fig. 2. During the mesh generation process, the maximum edge size for the elements around the soil-column interface was set to 0.15 m and the defined interface contact is demonstrated in Fig. 4(d). The isotropic Coulomb friction model available in Abaqus (2012) was used to simulate the soil-JGC interface behaviour and the frictional coefficient was assigned as 0.7 that was determined after the various trials of calibration. The model calibration process is undertaken considering the axial loading test result obtained from the unreinforced Bojszowy Nowe field trial column (Bzówka, 2009; Bzówka and Pieczyrak, 2008; Modoni and Bzowka, 2012) shown in Fig. 5. The initial stress condition and the parameters given in Table 2 and Fig. 2 are introduced to the analyses in order to reproduce the axial loading test results reported by Modoni and Bzowka (2012). In these 3D FE analyses the geometrical variation of column with depth is simulated by the rotated sinusoidal function given in Fig. 1(c) and the obtained load-settlement results are presented in Fig. 5. The figure also shows the previous results reported by Modoni and Bzowka (2012). Fig. 5 shows that the rotated sinusoidal functional prediction assumed in this paper that takes into account the local diameter variations provides better agreement with the field test results compared to that of the funnel-shaped functional prediction presented by Modoni and Bzowka (2012).

3. 3D FE Simulation of JGRs Subjected to Nonuniform Vertical Loading

The three main configurations shown in Fig. 6 are considered for the 3D FE simulation of JGR system in which the geometrical variation of JGCs with depth is represented by the rotated sinusoidal function. The presented numerical analyses have been performed to investigate the mutual interactions between the foundation elements under the nonuniform vertical loading.

3.1 Configuration of 3D FE Models

A square raft having the edge length of 9.0 m and the thickness of 0.5 m is assumed in the model configurations. Two loading areas on the rafts are defined as the core and the edge areas illustrated in Fig. 6. A core area of a raft is usually specified as 25% of the total raft area (Reul and Randolph, 2004) and the rest of the total raft area is named as edge area to simulate the simplified loading regime of rafts which generally support the elevator shafts and stairways at the centre area and columns at the edge area bearing the facade. The centre-to-centre column

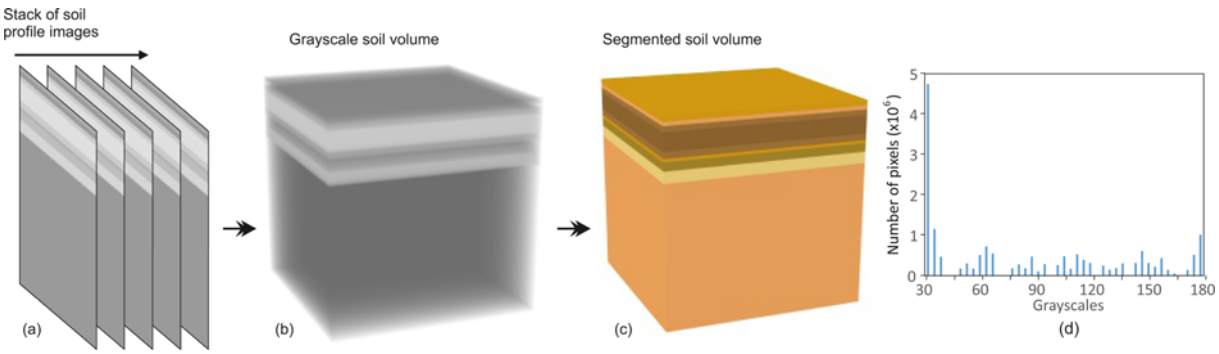

Fig. 3. Image Processing Stages Used in 3D FE Modelling: (a) the Soil Profile Images, (b) Grayscale Volume, (c) Segmented Volume, (d) the Grayscale Values

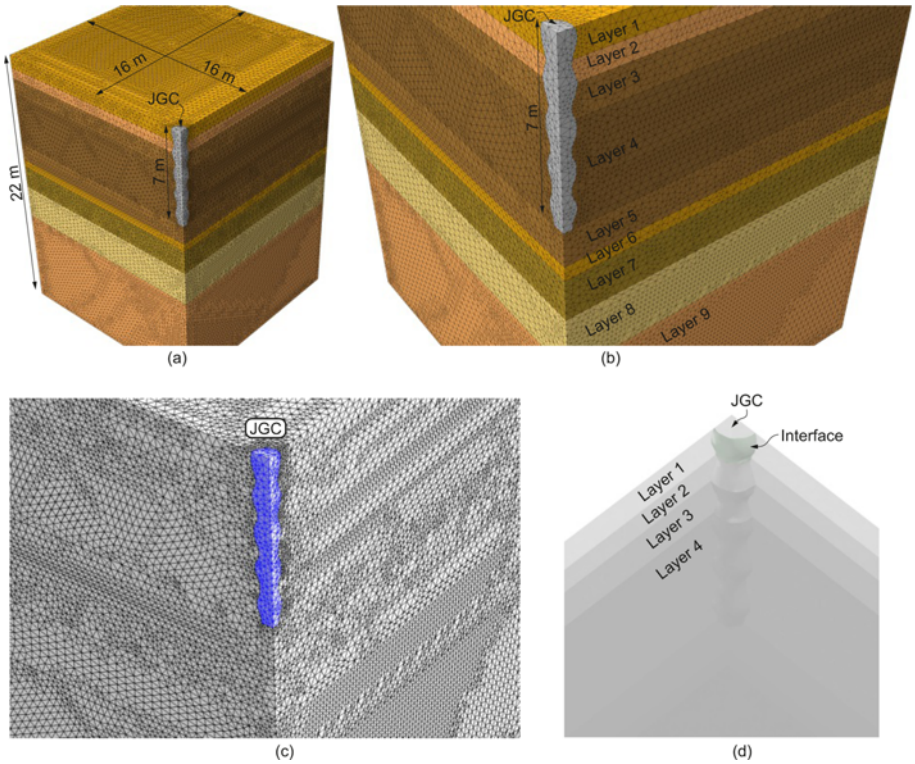

Fig. 4. 3D FE Mash of the Trial Columns Modelled using the Rotated Sinusoidal Function (illustrated in Fig. 1(c)), (a) the General View of the Mesh, (b) a Close-up View of the Column and Soil Layers, (c) a Close-up View of FE Mesh in Abaqus (2012), (d) a Close-up View of the Interface Contact

Table 2. Constitutive Parameters

Material	γ (kN/m^3)	$E_{50\%}$ (MPa)	E_{ur} (MPa)	ν	ϕ'(°)	c' (kPa)	ψ(°)
Soil (hardening soil)	18.4 ([a]) 19.2 ([b])	Fig. 2(b)	$3 \times E_{50}$	0.2	Fig. 2(a)	0	Fig. 2(a)
JG (Mohr Coulomb)	25	3200		0.19	0	4000	0
Raft (linear elastic)	25	33000		0.2			
Cushion (hardening soil)	24	40	$3 \times E_{50}$	0.2	37	0	7

([a]) above water level ([b]) below water level

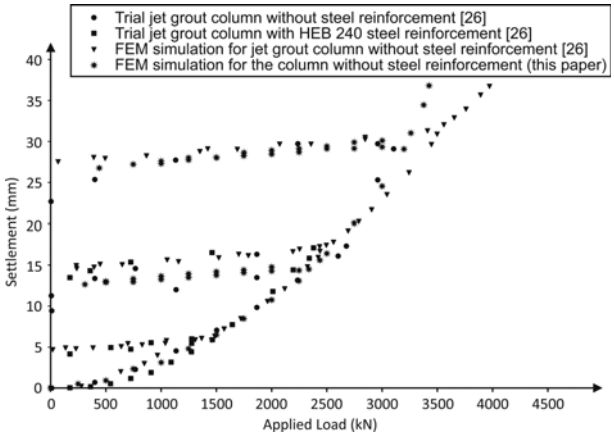

Fig. 5. The Experimental and Theoretical Load-settlement Results for the Trial Column

spacing assumed having a constant value is specified as 1.5 m, 2.25 m and 3 m in Configuration 1, 2 and 3, respectively (Fig. 6). JGC lengths of 6 m, 10 m and 14 m are considered in all configurations (Fig. 1(c) to 1(e)). The column length in the core area is taken greater than that of the edge area because the columns are generally used to control the settlement rather than to carry the entire load. The thickness of cushion layer is assumed as 0.25 m, 0.35 m and 0.55 m in all configurations. The geometrical variations of columns used in the 3D FE simulation of JGR systems are defined by the rotated sinusoidal function considered in the previous section (see Figs. 1(d)-1(f)). Fig. 7 shows the typical tetrahedral FE mesh developed for each configuration (Fig. 6) in which the previously introduced soil profile (Fig. 2) and image processing technique (Fig. 3) are used. For the sake of computational convenience, the quarter of the symmetrical model is used as demonstrated in Fig. 7 and the mash refinements are applied around the JGCs and raft. The model dimensions given in Fig. 7 are in good agreement with the many 3D FE models presented for the piled raft design (e.g. (Liang *et al.*, 2003; Reul and Randolph, 2004)).

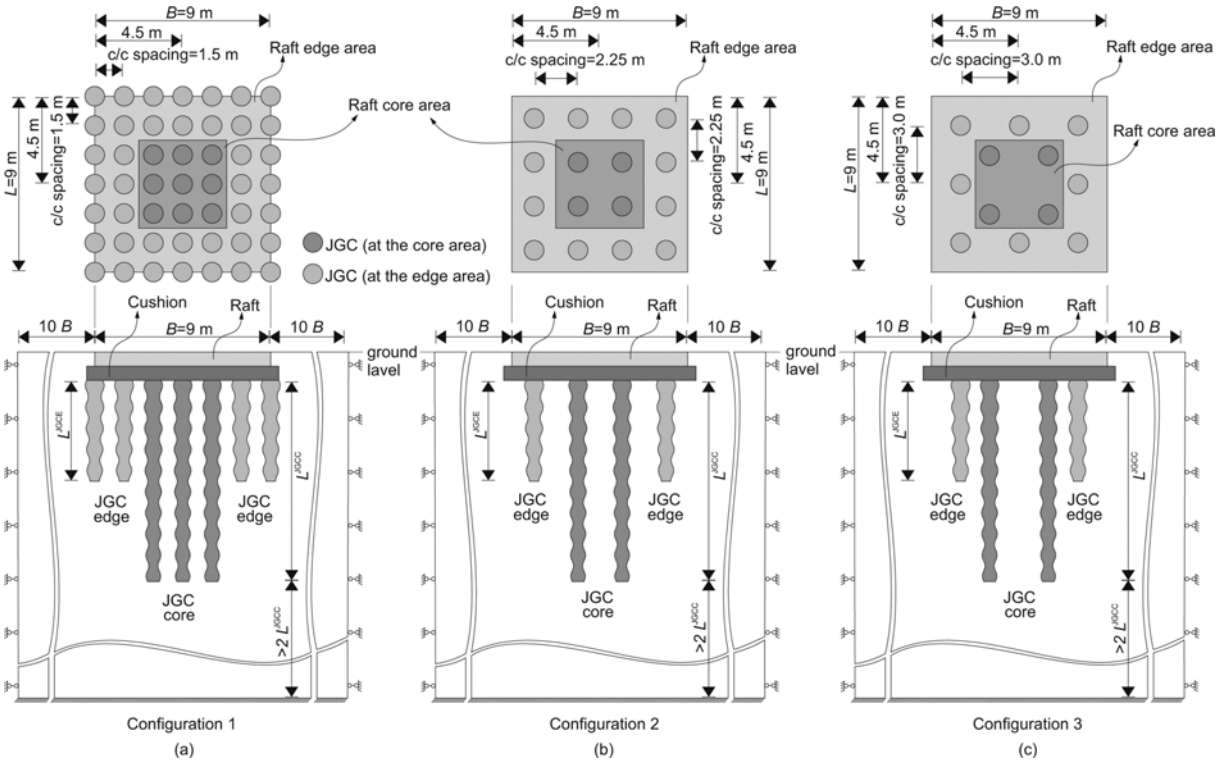

Fig. 6. The Configurations of JGR Subjected to Nonuniform Vertical Loading for Parametric Study

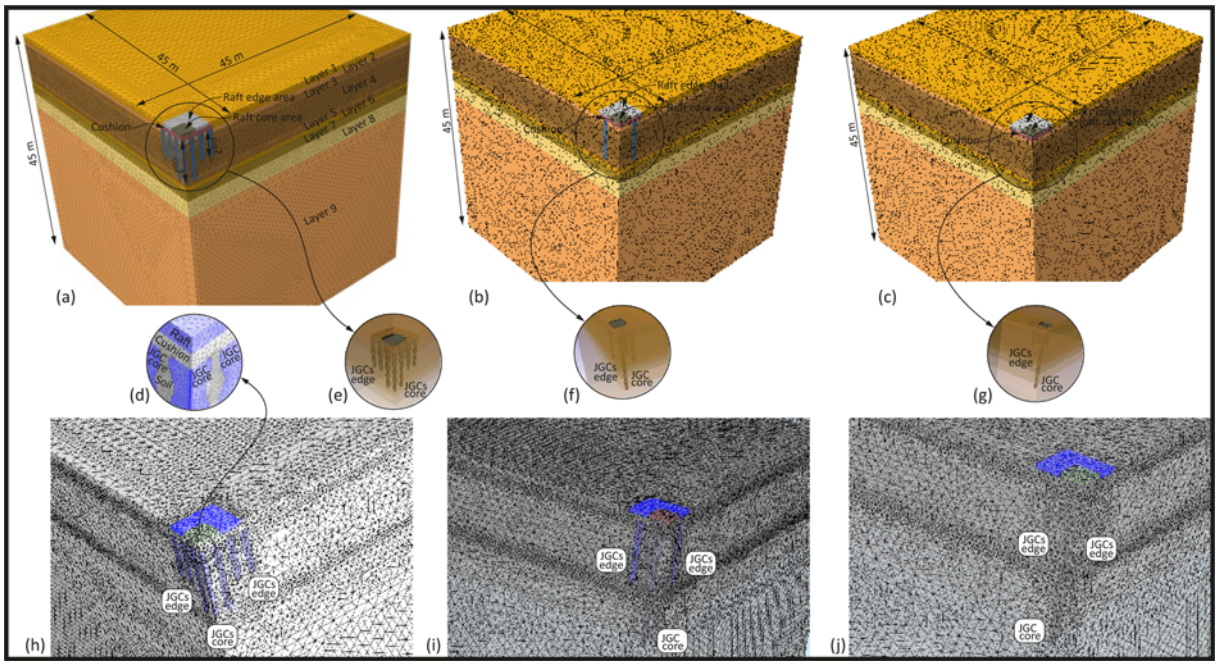

Fig. 7. Typical 3D FE Mashes Developed for Each Configuration Illustrated in Fig. 6

3.2 Constitutive Models

The constitutive model parameters adopted from Modoni and Bzowka (2012) are shown in Table 2 and Fig. 2 and utilised for the presented 3D FE models. These parameters have been obtained from the back-analysis of the results for the axial loading test reported by Modoni and Bzowka (2012). The stress-strain response of each sublayers demonstrated in Fig. 2 is simulated with a nonlinear hardening plasticity constitutive model (Schanz, 1998). Mohr–Coulomb elasto-plastic model is used for the columns and the behaviour of raft is assumed to be linear elastic (Modoni and Bzowka, 2012). The soil-column interface is defined to enable the relative displacements between

the column and surrounding soil as presented for the simulation of a single column. The maximum edge size for the tetrahedral element around the column was assigned as 170 mm pixel spacing and the defined interface between the column and the surrounding soil is shown in Fig. 4(d). The initial stress state for the soil is used with the gravity loading by introducing the Jaky's formula (1944). The nonuniform vertical loading is applied to the raft such that the pressures of 750 kPa and 1500 kPa are applied to the edge and core areas of raft, respectively.

3.3 Design Constraints of JGRs

The design parameters and constraints for the JGR systems have recently been defined by Algin (2016) by combining the previously defined design strategies for the piled rafts (Reul and Randolph, 2004) and JGCs (Croce *et al.,* 2014). The following three constraints previously defined by Reul and Randolph (2004) to design the piled rafts are adopted for the design of JGRs.

$$s_{ra}^{JG} \le \zeta_{asr}\, s_{ra} \tag{1}$$

$$\Delta s_r^{JG} \le \zeta_{\Delta sr}\, \Delta s_r \tag{2}$$

$$m_{r(\max)}^{JG} \le \zeta_{mr}\, m_{r(\max)} \tag{3}$$

The above average settlements for unpiled raft (S_{ra}) and JGR (S_{ra}^{JG}) can be calculated using the following approximation suggested by Davis and Taylor (1962).

$$s_{average} \approx \tfrac{1}{3}(2s_{center} + s_{corner}) \tag{4}$$

These coefficients (i.e. ζ_{asr}, $\zeta_{\Delta sr}$ and ζ_{mr}) directly indicate the performance of JGR are generally assumed to be smaller than 1 because the installation of JGCs should be beneficial. The previous research (Algin, 2016) has demonstrated that there are some arrangements of JGCs that result an increase in the design parameters (Eqs. (1) to (3)) such as the differential settlements compared to the raft without the columns. Therefore, it is worth to check these coefficients for the design of JGR to ensure that they are smaller than 1. Accordingly, these coefficients are used as the nondimensional design parameters (i.e. S_{ra}^{JG}/S_{ra}, $\Delta S_r^{JG}/\Delta S_r$ and $m_{r(\max)}^{JG}/m_{r(\max)}$).

Since Eurocode 7 (BS-EN-1994-1, 2004) assumes a limit settlement equal to 0.5% of the foundation base, this limitation is considered as a design constraint for JGRs. Therefore, the maximum average settlement of 0.045 m is assumed as an settlement constraint for the JGR configurations shown in Fig. 6. As to the limitation of differential settlement, it is defined as an ratio between the maximum differential settlement and the breadth of raft. Since this ratio should be smaller than 0.001 (e.g. (Reul and Randolph, 2004)), the maximum differential settlement of 0.009 m is assumed as a constraint for the JGR configurations shown in Fig. 6.

Several previous researchers (e.g. (Croce *et al*., 2014; Modoni and Bzowka, 2012)) have demonstrated that the applied load is transferred to the surrounding soil partly from the tip and partly from the lateral surface of JGCs. Modoni and Bzowka (2012) examined this mechanism to derive the load transfer curves along the lateral surface and the lower tip of JGCs using the back-analysing of the results from the axial loading tests performed on JGCs in sandy soil and by calibrating a FE model incorporated with the theoretical funnel-shape functional prediction.

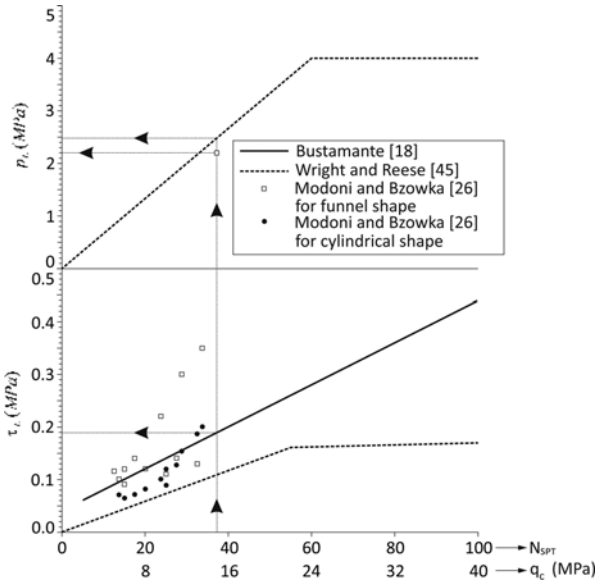

Fig. 8. The Ultimate Vertical Stress (τ_L) and the End-bearing Capacity (p_L)

The arrowed live in Fig. 8 demonstrates how the limiting values for the end-bearing capacity (p_L) and the ultimate vertical stresses (τ_L) can be obtained using the curves provided by Wright and Reese (1977) and Bustamante (2002) in terms of the average in situ test results. The value of 2.2 MPa for τ_L was previously calculated by Modoni and Bzowka (2012). It provides a good agreement with the value obtained from the curve of Wright and Reese (1977). Fig. 8 shows how the value of 0.189 MPa is obtained for τ_L as demonstrated by Algin (2016).

The secant Young modulus ($E_{50\%}$) for the columns can be obtained based on the following relationship suggested by Modoni and Bzowka (2012) using the uniaxial compressive strength (q_u) results.

$$E_{50\%} = \beta_E\, q_u \tag{5}$$

On the bases of the available data, the values for β_E and q_u are suggested as 400 and 8 MPa by Modoni and Bzowka (2012), respectively. Accordingly, the secant Young modulus shown in Table 2 are considered for the columns. These quantified constraints of 2.2 MPa, 0.189 MPa and 8 MPa for p_L, τ_L and q_u are finally divided by the partial safety factor of 1.3 as suggested by Annex A of Eurocode 7 (BS-EN-1994-1, 2004) to obtained the design values.

As suggested by Algin (2016) the maximum axial stress of the column can be limited with the uniaxial compressive strength of jet grouting material if the steel reinforcement is not required to be used in the columns. This is a reasonable constraint on the

Table 3. Assumed Costs for the Design Optimisation

	Unit	Approx. Price[+]
JGC[++]	USD($)/m	68.56[a]
Reinforced JGC[++]	USD($)/m	88.56[b]
Cushion[++]	USD($)/m^3	5.676[c]
Raft	Not included	

([a]) JGC construction + cement
([b]) JGC construction + cement + steel
([c]) Construction of compacted granular material
([+]) Unit prices are obtained from Turkish Ministry of Environment and Urban Planning Construction and Installation Unit Price List (2015) (http://www.birimfiyat.net/)
([++]) Material code numbers: Y.16.072/06, Y.16.050/06, Y.23.015, Y.15.140/03

steel reinforcement consideration for a safe design. If the maximum axial stress is greater than the uniaxial compressive strength of the column then the difference of stress should be sustained by the required steel reinforcement (Algin, 2016). Modoni and Bzowka (2012) also suggests to use the following equation to obtain the limit axial load that implies the possibility of reinforcement inclusion into the column.

$$S_{\lim} = \sigma_c a_c + \sigma_f a_f \tag{6}$$

The costs of design elements given in Table 3 are used in the presented cost-benefit studies on the JGR systems to determine the optimum design options that best meet the design criteria. These costs are only used for an academic purpose and may differ in terms of the project size, location, site conditions etc. Since the constant thickness of raft (Fig. 6) is used in this paper the cost for raft is excluded from the presented cost optimisation analyses.

3.4 Responses from the 3D FE Analyses

3D FE models developed using the various factors of cushion thickness, column spacing and length have been analysed using the FE analysis software Abaqus (2012). The obtained results of S_{ra}^{JG}, ΔS_r^{JG} and $m_{r(\max)}^{JG}$ from the numerical analyses are used to calculate the factors of ζ_{asr}, $\zeta_{\Delta sr}$ and ζ_{mr} (Eqs. (1)-(3)). Additionally, the design responses of $p_{\max}^{JGCC}$, $p_{\max}^{JGCE}$, $\tau_{\max}^{JGCC}$, $\tau_{\max}^{JGCE}$, $\sigma_{z(\max)}^{JGCC}$ and $\sigma_{z(\max)}^{JGCE}$ are obtained from the numerical analyses for the columns under the core and edge areas of rafts. The costs are calculated for each configuration. The aforementioned steel reinforcement requirement is determined for the columns under the core and edge areas. The cross-sectional area is calculated using Eq. (6) and it is determined that the steel bar reinforcement having the diameter of 60 mm is adequate for all of the cases.

Figure 9 shows that the axial stress, the vertical stress at the base and the vertical stress on the shaft under the core area are higher than that of the edge area for the column spacing of 1.5 m, 2.25 m and 3 m (Figs. 6). The figure show that the axial stress is greater for the high values of column spacing. Fig. 9(a) also shows that the axial stress is increased as the maximum value of 20% when the column length under the core area is increased from 6 m to 14 m. Fig. 9(b) indicates that the increase in the column length under the core area decreases the vertical stress at the base as much for the common observation indicated that high loads are transferred from the lateral surface of the columns to the surrounding soil (Garassino, 1997; Maertens and Maekelberg, 2001). The maximum reduction in the vertical stress at the base is approximately 15% when the column length under the core area is increased from 6 m to 14 m. Fig. 9(c) indicates that approximately 40% reduction in vertical shaft stresses is obtained when the column length under the core area is increased from 6 m to 14 m. Fig. 10 demonstrates some of the obtained values for the coefficients of ζ_{asr}, $\zeta_{\Delta sr}$ and ζ_{mr} in relation with the variation of column length in the core area and the column spacing. The figure show that the highest reduction is observed for the differential settlement. For instance the reduction of ζ_{asr}, $\zeta_{\Delta sr}$ and ζ_{mr} for Combination 2 is approximately 20%, 58% and 40%, respectively, when the column lengths of 6 m and 14 m are compared. Fig. 11 shows the coefficients of ζ_{asr}, $\zeta_{\Delta sr}$ and the axial stress of columns under the edge area in relation with the variation of cushion thickness and the column length in the core and edge areas for the column spacing of 2.25 m.

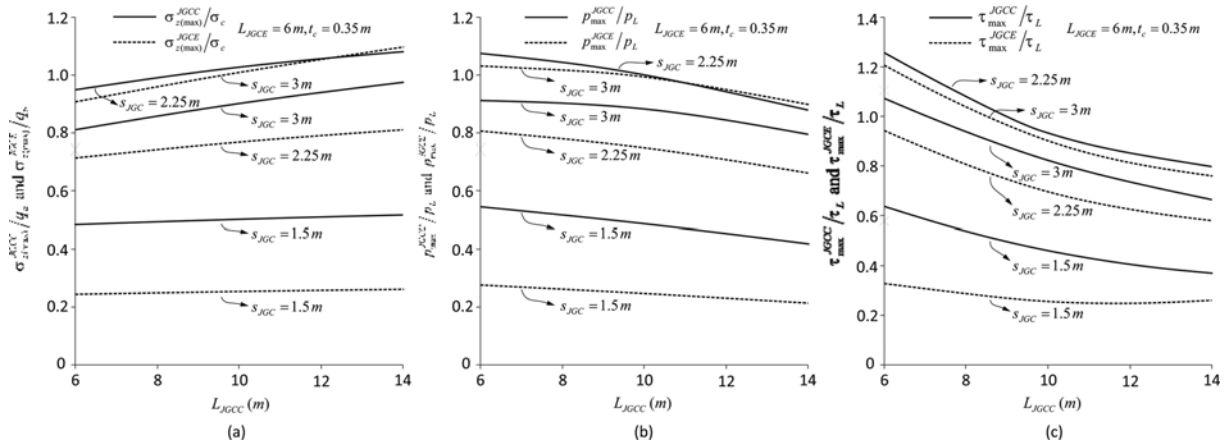

Fig. 9. Influence of the Column Length on the Axial Stress, the Vertical Stress at the Base and the Vertical Stress on the Shaft of Columns Under the Core and Edge Areas: (a) the Axial Stress, (b) the Vertical Stress at the Base, (c) the Vertical Stress on the Shaft

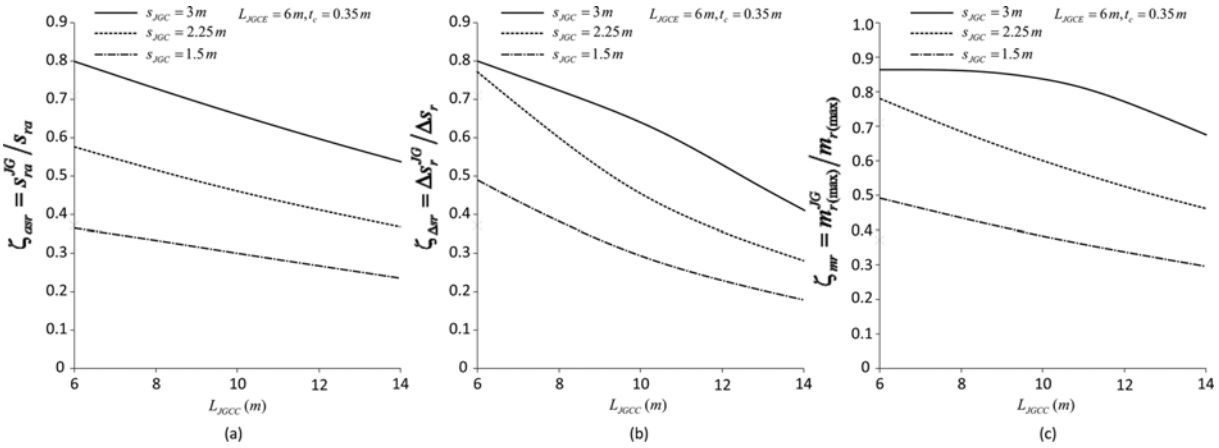

Fig. 10. Influence of the Column Length on the Design Coefficients: (a) the Average Settlement Coefficient, (b) the Differential Settlement Coefficient, (c) the Maximum Bending Moment Coefficient

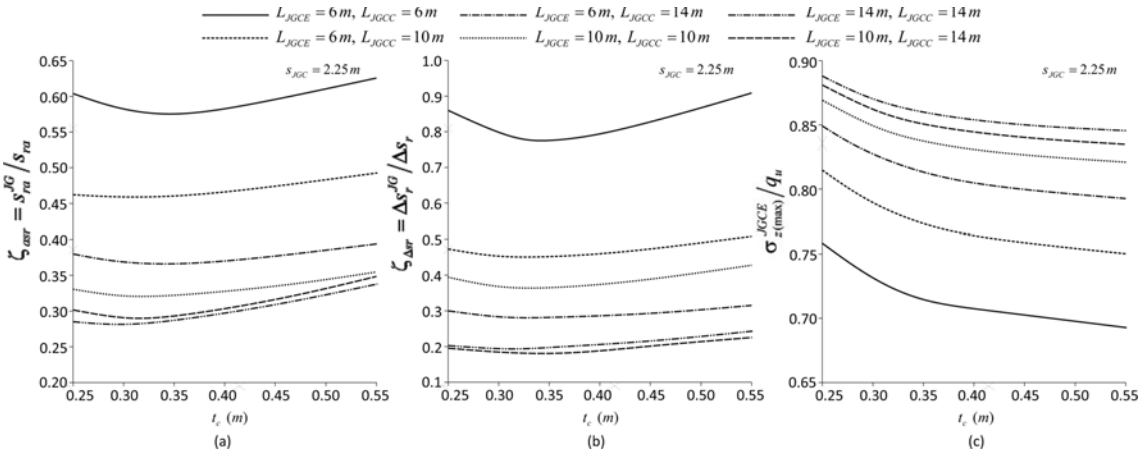

Fig. 11. Influence of the Cushion Thickness on the Axial Stress and the Design Coefficients: (a) the Average Settlement Coefficient, (b) the Differential Settlement Coefficient, (c) the Axial Stress

3.5 Statistical Analysis of the Results

The general linear model analysis of variance (ANOVA) at 95% confidence level has been conducted to determine the statistical significance of the design factors on the responses. In this paper, the parameters of S_{JGC}, t_c, L_{JGCC} and L_{JGCE} are considered as the design factors and the design responses are defined as $p_{\max}^{JGCC}$, $p_{\max}^{JGCE}$, $\tau_{\max}^{JGCC}$, $\tau_{\max}^{JGCE}$, $\sigma_{z(\max)}^{JGCC}$, $\sigma_{z(\max)}^{JGCE}$, S_{ra}^{JG}, Δs_r, $m_{r(\max)}$, ζ_{asr}, $\zeta_{\Delta sr}$, ζ_{mr}, and *Cost*. ANOVA is also performed to identify the level of effectiveness of the independent variables on the design responses. Table 4 shows the obtained *p*-values for which if it is higher than 0.05, the parameter is rejected as an insignificant factor on the response at 95% confidence level.

All of the independent variables are determined to be statistically significant except the factor of t_c due to the fact that the cost of cushion is less influential than the cost of columns. The contribution level of the design factors on the responses are also demonstrated in Table 4. The higher the percentage contribution is the higher the effectiveness of factors on that particular response. Table 4 shows that the column spacing is the most crucial design factor for the responses of $p_{\max}^{JGCE}$, $p_{\max}^{JGCC}$, $\tau_{\max}^{JGCE}$, $\sigma_{z(\max)}^{JGCE}$, $\sigma_{z(\max)}^{JGCC}$, S_{ra}^{JG}, $m_{r(\max)}^{JG}$, ζ_{asr}, ζ_{mr} and *Cost*. It also demonstrates that the column length under the core area is the most influential factor on the responses of $\tau_{\max}^{JGCC}$, ΔS_r^{JG} and $\zeta_{\Delta sr}$. It is also determined that the column length under edge area is highly effective on $p_{\max}^{JGCC}$, $p_{\max}^{JGCE}$, $\tau_{\max}^{JGCE}$, $m_{r(\max)}^{JG}$, ζ_{mr} *Cost*. The influence of cushion thickness is higher for $p_{\max}^{JGCC}$ and minimal for the other responses. It can also be observed from Table 4 that the column length under the core area is more effective than that of the length under the edge area for $\tau_{\max}^{JGCC}$, S_{ra}^{JG}, ΔS_r^{JG}, $m_{r(\max)}^{JG}$, ζ_{asr}, $\zeta_{\Delta sr}$ and ζ_{mr}. The agreement between this outcome and the results from some studies on piled rafts is relatively satisfactory as much for the settlements (e.g. (Horikoshi and Randolph, 1998; Reul and Randolph, 2004)).

4. Optimization Analysis

The presented multi objective optimization analysis is performed using the Response Surface Method (RSM) (Whitcomb and Anderson, 2004). RSM combines mathematical and statistical methods of experiment design, regression analysis and optimization.

Table 4. ANOVA Results for the Considered Responses

Dependent Variables	Source of variation	Statistical parameters					Significant	Contribution (PC_x) (%)	Dependent Variables	Source of variation	Statistical parameters					Significant	Contribution (PC_x) (%)
		Degree of freedom (df)	Sum of square (SS_x)	Mean square (MS_x)	F	P-value					Degree of freedom (df)	Sum of square (SS_x)	Mean square (MS_x)	F	P-value		
$p_{\max}^{JGCE}$	s_{JGC}	2	1.40E+07	7089788	134.6	0.0000	Yes	70.07	ΔS_r^{JG}	s_{JGC}	2	0.00015	7.70E-05	112.57	0.0000	Yes	36.95
	L_{JGCE}	2	4625157	2312579	43.9	0.0000	Yes	22.85		L_{JGCE}	2	1.80E-05	9.20E-06	13.45	0.0000	Yes	4.42
	L_{JGCC}	2	1013543	506771	9.62	0.0000	Yes	5.01		L_{JGCC}	2	0.00024	0.00012	174.17	0.0000	Yes	57.17
	t_c	2	418905	209452	3.98	0.0260	Yes	2.07		t_c	2	6.10E-06	3.00E-06	4.45	0.0170	Yes	1.46
	Error	45	2370299	52673						Error	45	3.10E-05	7.00E-07				
$p_{\max}^{JGCC}$	s_{JGC}	2	7058951	3529475	117.3	0.0000	Yes	44.92	$m_{r(\max)}^{JG}$	s_{JGC}	2	414560	207280	330.59	0.0000	Yes	72.98
	L_{JGCE}	2	6584325	3292163	109.42	0.0000	Yes	41.90		L_{JGCE}	2	63133	31566	50.35	0.0000	Yes	11.12
	L_{JGCC}	2	1496335	748168	24.87	0.0000	Yes	9.52		L_{JGCC}	2	82498	41249	65.79	0.0000	Yes	14.52
	t_c	2	573490	286745	9.53	0.0000	Yes	3.65		t_c	2	7815	3908	6.23	0.0040	Yes	1.38
	Error	45	1353978	30088						Error	45	28215	627				
$\tau_{\max}^{JGCE}$	s_{JGC}	2	336932	168466	351.04	0.0000	Yes	75.74	ζ_{asr}	s_{JGC}	2	0.96984	0.48492	355.11	0.0000	Yes	75.59
	L_{JGCE}	2	79869	39935	83.21	0.0000	Yes	17.95		L_{JGCE}	2	0.10298	0.05149	37.71	0.0000	Yes	8.03
	L_{JGCC}	2	20524	10262	21.38	0.0000	Yes	4.61		L_{JGCC}	2	0.19441	0.09721	71.18	0.0000	Yes	15.15
	t_c	2	7542	3771	7.86	0.0010	Yes	1.70		t_c	2	0.01572	0.00786	5.76	0.0060	Yes	1.23
	Error	45	21596	480						Error	45	0.06145	0.00137				
$\tau_{\max}^{JGCE}$	s_{JGC}	2	76979	38490	200.94	0.0000	Yes	44.14	$\zeta_{\Delta sr}$	s_{JGC}	2	0.64675	0.32338	112.57	0.0000	Yes	36.95
	L_{JGCE}	2	12108	6054	31.61	0.0000	Yes	6.94		L_{JGCE}	2	0.07729	0.03865	13.45	0.0000	Yes	4.42
	L_{JGCC}	2	82281	41141	214.78	0.0000	Yes	47.18		L_{JGCC}	2	1.0007	0.50035	174.17	0.0000	Yes	57.17
	t_c	2	3040	1520	7.93	0.0010	Yes	1.74		t_c	2	0.02555	0.01278	4.45	0.0170	Yes	1.46
	Error	45	8620	192						Error	45	0.12927	0.00287				
$\sigma_{z(\max)}^{JGCE}$	s_{JGC}	2	4.20E+08	2.10E+08	1854.61	0.0000	Yes	98.51	ζ_{mr}	s_{JGC}	2	1.29091	0.64546	330.59	0.0000	Yes	72.98
	L_{JGCE}	2	2016069	1008035	8.89	0.0010	Yes	0.47		L_{JGCE}	2	0.19659	0.0983	50.35	0.0000	Yes	11.12
	L_{JGCC}	2	2816554	1408277	12.43	0.0000	Yes	0.66		L_{JGCC}	2	0.25689	0.12845	65.79	0.0000	Yes	14.52
	t_c	2	1505398	752699	6.64	0.0030	Yes	0.35		t_c	2	0.02434	0.01217	6.23	0.0040	Yes	1.38
	Error	45	5099719	113327						Error	45	0.08786	0.00195				
$\sigma_{z(\max)}^{JGCC}$	s_{JGC}	2	2.10E+08	1.00E+08	1433.32	0.0000	Yes	96.42	Cost	s_{JGC}	2	4.50E+09	2.30E+09	239.11	0.0000	Yes	83.19
	L_{JGCE}	2	2408559	1204280	16.47	0.0000	Yes	1.11		L_{JGCE}	2	8.20E+08	4.10E+08	43.71	0.0000	Yes	15.21
	L_{JGCC}	2	3387953	1693977	23.17	0.0000	Yes	1.56		L_{JGCC}	2	8.70E+07	4.30E+07	4.59	0.0150	Yes	1.60
	t_c	2	1983186	991593	13.56	0.0000	Yes	0.91		t_c	2	33673	16836	0	0.9980	No	0.00
	Error	45	3290281	73117						Error	45	4.20E+08	9422394				
S_{ra}^{JG}	s_{JGC}	2	0.01167	0.00584	355.11	0.0000	Yes	75.59									
	L_{JGCE}	2	0.00124	0.00062	37.71	0.0000	Yes	8.03									
	L_{JGCC}	2	0.00234	0.00117	71.18	0.0000	Yes	15.15									
	t_c	2	0.00019	9.50E-05	5.76	0.0060	Yes	1.23									
	Error	45	0.00074	1.60E-05													

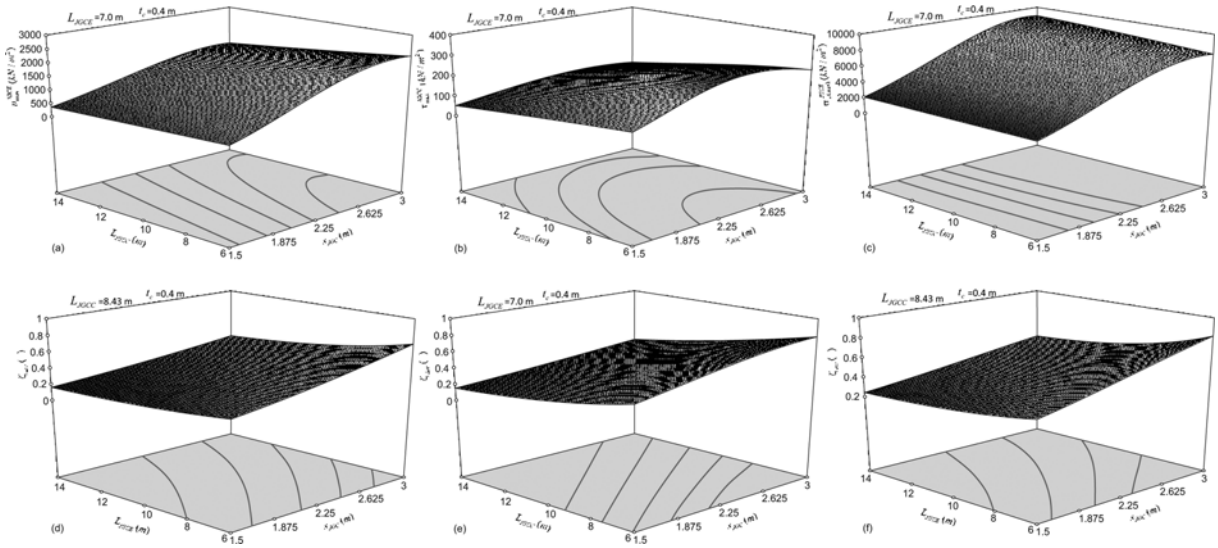

Fig. 12. The Effects of Design Factors on the Responses: (a) the Vertical Stress at the Base, (b) the Vertical Stress on the Shaft, (c) the Axial Stress, (d) the Average Settlement Coefficient, (e) the Differential Settlement Coefficient, (f) the Maximum Bending Moment Coefficient

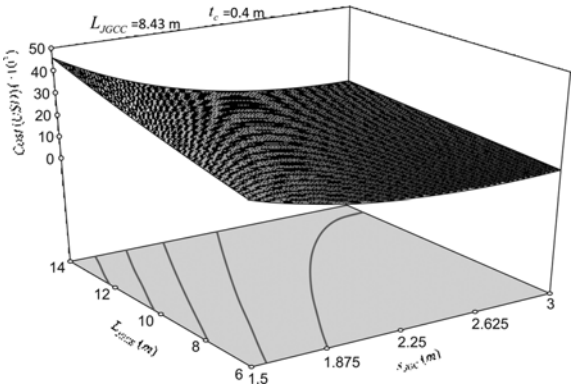

Fig. 13. The Effect of Column Spacing and Length on the Response of Cost

Table 5. Definitions of Factors and Responses Used in the Optimization Process

Names		Goal	Lower Limit[a]	Upper Limit[a]	
Factors	s_{JGC}	is in range	1.5	3	
	L_{JGCE}	is in range	6	14	
	L_{JGCC}	is in range	6	14	
	t_c	is in range	0.25	0.55	
Responses	p_{max}^{JGCE}	is in range	110.88	1692.31	(Constrained)
	p_{max}^{JGCC}	is in range	219.03	1692.31	(Constrained)
	τ_{max}^{JGCE}	is in range	31.2	145.38	(Constrained)
	τ_{max}^{JGCC}	is in range	44.74	145.38	(Constrained)
	$\sigma_{z(max)}^{JGCE}$	is in range	1901.04	6153.85	(Constrained)
	$\sigma_{z(max)}^{JGCC}$	is in range	3755.15	6153.85	(Constrained)
	s_{ra}^{JG}	is in range	0.0203	0.045	(Constrained)
	Cost	is in range	6491.26	47285.03	
	ΔS_r^{JG}	is in range	0.0018	0.009	(Constrained)
	$m_{r(max)}^{JG}$	is in range	125.97	521.16	
	ζ_{asr}	is in range	0.1852	0.8637	(checked)
	$\zeta_{\Delta sr}$	is in range	0.1196	0.9081	(checked)
	ζ_{mr}	is in range	0.2223	0.9197	(checked)

[a] Units are in kN, m and Cost is in USD($)

In this method, the regression analysis is undertaken for each response and the relationships between the independent variables and the responses are defined by the regression models that are included the combined binary effects of the independent variables. Additional ANOVA is undertaken to make sure that the statistically significant terms are included in each regression model. Power, square root or logarithmic transpositions are applied if required to enhance the regression models. The full quadratic model is mostly used by introducing the backward technique at $\alpha = 0.05$ level. The more detailed explanation of RSM is provided in the previous study (Algin, 2016). Figs. 12 and 13 demonstrate the 3D plots for the numerical variation of some regression models developed. In this optimization process, the optimum values for the design factors (i.e. column spacing, cushion thickness, the column lengths in the core and edge areas) are targeted while minimizing the construction cost by complying with the design constraints and parameters. Accordingly, the

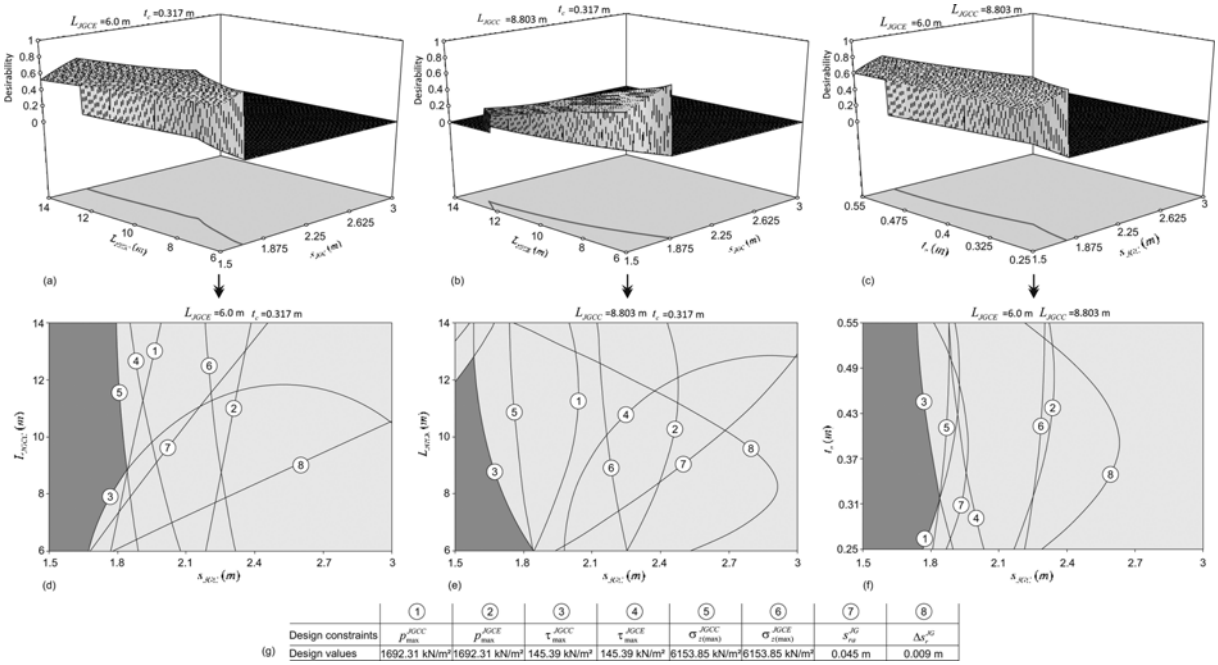

Fig. 14. Variation of Desirability in Terms of the Column Spacing and: (a) the Column Length Under the Core Area, (b) the Column Length Under the Edge Area, (c) the Cushion Thickness; and the Influence of the Design Parameters and Constraints on the 2D Plot Axes,(d) the Column Length Under the Core Area, (e) the Column Length Under the Edge Area, (f) the Cushion Thickness

multi objective optimization analysis technique using RSM is undertaken by considering the desirability functions defined for each target response (e.g. (Güneyisi *et al*., 2014; Pradeep, 2008; Whitcomb and Anderson, 2004)). Desirability is an objective function ranging from zero (i.e. it is outside the range) to one (viz. the goal has been achieved). All of the target responses are combined into a desirability function following the RSM procedure (Myers *et al.*, 2009). The factors and responses are defined as in Table 5 for the simultaneous multi-objective optimization process.

Two optimisation analyses have been conducted separately. In the first analysis, the axial stress ($\sigma_{z(\max)}^{JGCC}$) is constrained with the design value of uniaxial compressive strength of jet grouting material (Table 5). This approach indicates that the steel reinforcement is not required to be used in JGCs. Table 6 shows the first 10 optimum solutions and Fig. 14 demonstrates the variation of desirability function obtained from this optimisation analysis. In the second optimisation analysis, the limitation of axial stress is removed to be able to consider the use of the steel reinforcement in the design scenarios if required. Table 7 shows the first 10 optimum solutions from this optimization analysis. The provided optimum solutions in Tables 6 and 7 satisfy the defined upper and lower limits and demonstrate high desirability values ranging from 0.8203 to 0.8187 and 0.8380 to 0.8338, respectively.

Figures 14(a) to 14(c) show the 3D plot of desirability function varies in terms of design factors for the first solution provided in Table 6. Figs. 14(d) to 14(f) demonstrate the corresponding 2D overlap plots which are the projection of the desirability surface on the axes indicating factors. Figs. 14(g) provides a legend for the values of constraints and the corresponding notations are used to demonstrate their restricting effects on the overlap plots (Figs. 14(d)-14(f)). These constraining lines shown in Figs. 14(d) to 14(f) affects the desirability surface indicating the possible optimum solutions exist in the design optimisation. The observation of these constraining lines shows that the limiting values of $\tau_{\max}^{JGCC}$, $\sigma_{z(\max)}^{JGCC}$ and $p_{\max}^{JGCC}$ (corresponding the lines of 3, 5 and 1, respectively) are more dominant and important on the optimum solutions at the projection axes, the average settlement limitation is more effective than the differential settlement constraining value, the effects of the constraining values for ΔS_r^{JG} and $\tau_{\max}^{JGCE}$ on the optimum solutions are in the intermediate level and the design constraints for $p_{\max}^{JGCE}$ and $\sigma_{z(\max)}^{JGCE}$ indicate a minimal effect on the optimised design solutions of JGR system (Figs. 14(d)-14(f)). The figures also indicate that the constraints for $\tau_{\max}^{JGCC}$, S_{ra}^{JG} and ΔS_r^{JG} predominantly affect the optimisations of S_{JGC} whereas, the constraining values for $p_{\max}^{JGCC}$, $p_{\max}^{JGCE}$, $\tau_{\max}^{JGCE}$, $\sigma_{z(\max)}^{JGCC}$ and $\sigma_{z(\max)}^{JGCE}$ mostly influence the optimisations of JGC lengths under core and edge areas of raft.

Table 6 show that if the steel reinforcement is not required to be used for the JGCs, the most economical design solution

Table 6. Optimum Solutions of the JGR Subjected to Nonuniform Vertical Loading for in the Case of the Steel Reinforcement is Not Required

	Factors*				Responses*													Desirability
	s_{JGC}	L_{JGCE}	L_{JGCC}	t_c	$p_{\max}^{JGCE}$	$p_{\max}^{JGCC}$	$\tau_{\max}^{JGCE}$	$\tau_{\max}^{JGCC}$	$\sigma_{z(\max)}^{JGCE}$	$\sigma_{z(\max)}^{JGCC}$	S_{ra}^{JG}	Δs_r^{JG}	$m_{r(\max)}^{JG}$	ζ_{asr}	$\zeta_{\Delta sr}$	ζ_{mr}	Cost	
Solutions	1.841	6.000	8.832	0.320	1019.79	1687.45	119.33	145.38	3718.9	6153.84	0.0425	0.0065	284.40	0.3870	0.4206	0.5019	13823.5	0.8203
	1.843	6.000	8.925	0.329	1011.76	1672.33	121.13	145.35	3722.6	6153.09	0.0422	0.0064	282.10	0.3843	0.4133	0.4978	13836.7	0.8199
	1.844	6.000	8.962	0.332	1008.79	1666.50	121.92	145.38	3725.1	6153.82	0.0421	0.0063	281.25	0.3833	0.4106	0.4963	13837.9	0.8199
	1.848	6.000	9.147	0.352	993.70	1637.76	125.74	145.32	3733.8	6153.83	0.0415	0.0061	277.26	0.3787	0.3978	0.4893	13858.8	0.8194
	1.852	6.000	9.271	0.366	983.81	1618.82	128.48	145.32	3739.8	6153.84	0.0413	0.0060	274.97	0.3760	0.3903	0.4852	13870.7	0.8191
	1.843	6.017	8.957	0.331	1007.65	1665.43	121.58	145.38	3722.9	6153.26	0.0420	0.0063	280.77	0.3826	0.4102	0.4955	13880.7	0.8189
	1.846	6.013	9.062	0.342	999.42	1649.41	123.78	145.38	3728.7	6153.84	0.0417	0.0062	278.57	0.3801	0.4029	0.4916	13881.0	0.8188
	1.850	6.000	9.248	0.361	986.05	1623.72	127.56	144.98	3736.8	6153.37	0.0413	0.0060	275.32	0.3764	0.3917	0.4858	13884.0	0.8188
	1.856	6.000	9.431	0.388	971.33	1594.82	132.30	145.37	3748.0	6153.83	0.0410	0.0059	272.60	0.3733	0.3822	0.4810	13885.2	0.8187
	1.857	6.000	9.480	0.395	967.73	1587.86	133.51	145.38	3750.5	6153.84	0.0409	0.0059	272.07	0.3728	0.3802	0.4801	13888.9	0.8187

(*) Units are in kN, m and Cost is in USD($)

Table 7. Optimum Solutions of the JGR Subjected to Nonuniform Vertical Loading in the Case of the Steel Reinforcement is Required

	Factors*				Responses*													Desirability
	s_{JGC}	L_{JGCE}	L_{JGCC}	t_c	$p_{\max}^{JGCE}$	$p_{\max}^{JGCC}$	$\tau_{\max}^{JGCE}$	$\tau_{\max}^{JGCC}$	$\sigma_{z(\max)}^{JGCE}$	$\sigma_{z(\max)}^{JGCC}$	s_{ra}^{JG}	Δs_r^{JG}	$m_{r(\max)}^{JG}$	ζ_{asr}	$\zeta_{\Delta sr}$	ζ_{mr}	Cost	
Solutions	1.915	6.000	9.846	0.367	1062.02	1690.20	144.28	145.38	4135.9	6582.25	0.0415	0.0058	275.15	0.3780	0.3767	0.4855	13098.3	0.8380
	1.918	6.000	9.958	0.366	1064.56	1691.42	145.38	143.90	4162.4	6613.40	0.0413	0.0057	273.87	0.3764	0.3724	0.4833	13106.1	0.8378
	1.911	6.000	9.793	0.363	1061.28	1692.31	142.76	145.38	4116.6	6564.33	0.0415	0.0058	275.60	0.3784	0.3788	0.4863	13129.9	0.8373
	1.914	6.004	9.890	0.378	1050.35	1672.93	145.38	145.38	4117.2	6557.63	0.0413	0.0058	273.86	0.3763	0.3734	0.4833	13152.3	0.8367
	1.910	6.000	9.887	0.384	1041.42	1661.81	145.29	145.38	4088.9	6524.66	0.0412	0.0058	273.44	0.3758	0.3727	0.4825	13201.6	0.8355
	1.901	6.000	9.667	0.356	1055.68	1692.31	139.20	145.38	4060.4	6509.09	0.0416	0.0059	276.46	0.3792	0.3835	0.4879	13227.8	0.8349
	1.908	6.000	9.897	0.388	1034.94	1653.36	145.38	145.28	4071.7	6504.71	0.0412	0.0057	272.95	0.3751	0.3717	0.4817	13242.8	0.8345
	1.913	6.000	10.066	0.372	1048.25	1670.62	145.38	141.84	4126.8	6577.05	0.0409	0.0056	271.08	0.3728	0.3659	0.4784	13259.0	0.8341
	1.912	6.000	10.061	0.355	1061.71	1692.30	143.33	140.53	4147.3	6610.57	0.0410	0.0057	271.77	0.3736	0.3680	0.4796	13260.5	0.8341
	1.916	6.000	10.198	0.359	1059.47	1685.39	145.38	139.20	4170.6	6634.52	0.0407	0.0056	269.94	0.3714	0.3621	0.4763	13272.3	0.8338

(*) Units are in kN, m and Cost is in USD($)

having the design variables with 0.8203 desirability (the corresponding cost is 13823.5 USD) is obtained for the design factors of S_{JGC} = 1,841 m, L_{JGCE} = 6.0 m, L_{JGCC} = 8.832 m and t_c = 0.32 m. If the designer decides to insert ϕ60 mm steel bar as a reinforcement into JGCs under the core area, the optimum solution becomes S_{JGC} = 1.915 m, L_{JGCE} = 6.0 m, L_{JGCE} = 9.846 m and t_c = 0.367 m with 0.8380 desirability (the corresponding cost is 13098.3 USD) (Table 7). In case of steel reinforcements, the maximum bending moment of JGC with steel reinforcement should additionally be calculated and compared with the design value using the methods summarised by Croce *et al.* (2014). The above comparison clearly demonstrates that the inserting steel reinforcement provides more economical design solution if it is required.

5. Conclusions

The following conclusions may be drawn based on the key findings from the presented parametric study.

1. The rotated sinusoidal function presented for the geometrical representation of JGC is in a good agreement with both the theoretical funnel-shaped function and the measured data range. This function considers the local variation of column diameter and it is used in the 3D FE simulation of jet-grouted columns. It can easily be adjusted to the measured data and yields the general trend of the diameter reduction in depth. 3D FE analysis of a single JGC that is simulated by using the rotated sinusoidal function and the data from the axial loading test previously conducted provides better approximation especially for the higher applied loads.
2. The presented image processing technique used in 3D FE modelling allows the complex geometry of JGC to be modelled with the local diameter variation. This paper concludes that, in practice, this technique can therefore be utilised for the FE modelling of JGCs and JGR systems in order for accurately representing the measured trial JGC geometrical variation in the jet-grouted foundation projects.
3. The maximum axial stress increases with an increase in the column spacing. The increase in the column length under the core area decreases the vertical stress at the base. The maximum reduction in the vertical stress at the base is approximately 15% when the column length under the core area is increased from 6 m to 14 m. Approximately 40% reduction in vertical shaft stresses is obtained when the column length under the core area is increased from 6 m to 14 m.
4. Among the considered design factors, column spacing is generally the most important factor for the responses. The column length under the core area is determined to be the most effective factor on the maximum vertical shaft stress of the columns under the core area and the settlements of raft. However, the variation of column length under the core area is more influential on the differential settlement response than the column length under the edge area.
5. Paper concludes that RSM provides a useful approach to determine the optimum design of JGR systems. The design constraints for the maximum values of vertical shaft stress, axial stress and vertical stress at the base of JGCs under the core area have been determined to be more dominant and important on the optimum solutions of JGR subjected to nonuniform vertical loading. The average settlement limitation is more effective than the differential settlement constraining value, the effects of the constraining values for the differential settlement and the maximum value of vertical shaft stress of JGCs under the edge area are in the intermediate level and the design constraints for the maximum value of axial stress and vertical stress at the base of JGCs under the edge area indicate a minimal effect on the optimised design solutions of JGR system. The constraints for the maximum value of vertical shaft stress of JGCs under the core area and the settlements of raft predominantly affect the optimisation of JGC spacing whereas, the optimisation of JGC lengths under core and edge areas of raft is mostly affected by the constraining design values for the maximum values of axial stress and vertical stress at the base of JGCs under the core and edge areas, and the vertical shaft stress of JGCs under the edge area of raft.
6. The inserting steel reinforcement provides more economical design solution if it is required.

Notations

The symbols are used in this paper as follows:

a_c = Cross-sectional area at a generic section of column
a_f = Cross-sectional area for the steel reinforcement
B = Breadth of raft
c' = Cohesion of soil
E_c = Young's modulus for the cushion
E_{JG} = Young's modulus for the jet-grouted column
E_{ur} = Unloading modulus
$E_{50\%}$ = Secant modulus
K_n = Normal stiffness modulus of interface
K_t = Shear stiffness modulus of interface
L_{JGCE} = Length of column under the raft edge area
L_{JGCC} = Length of column under the raft core area
$m_{r(\max)}$ = Maximum bending moment of raft without the column system
$m_{r(\max)}^{JG}$ = Maximum bending moment of jet-grouted raft
p = Vertical stress at the column's base
$p_{\max}^{JGCE}$ = Maximum p value of the columns under the raft edge area
$p_{\max}^{JGCC}$ = Maximum p value of the columns under the raft core area
p_L = Limit value of p
q_c = Tip unit resistance of CPTs
q_u = Uniaxial compressive strength of the jet-grouted material
S, $S_{\lim}$ = Axial load and its limit value at a generic section of the column

S_{JGC} = Centre to centre column spacing
S_{ra} = Average settlement of raft without the column system
S_{rd} = Average settlement of jet-grouted raft
t_c = Thickness of the cushion
γ = Unit weight
γ' = Buoyant unit weight
Δs_r = Differential settlement of raft without the column system
ΔS_r^{JG} = Differential settlement of jet-grouted raft
ν = Poisson's ratio
σ_c = Uniaxial compression strength at a generic section of the column
σ_f = Compression strength of the steel reinforcement
$\sigma_{z(\max)}^{JGCE}$ = Maximum axial stress of the columns under the raft edge area
$\sigma_{z(\max)}^{JGCC}$ = Maximum axial stress of the columns under the raft core area
τ = Vertical stress on the shaft of the column
$\tau_{\max}^{JGCE}$ = Maximum τ value of the columns under the raft edge area
$\tau_{\max}^{JGCC}$ = Maximum τ value of the columns under the raft core area
τ_L = Limit value of τ
ζ_{ars} = Coefficient for average settlement of jet-grouted raft
$\zeta_{\Delta sr}$ = Coefficient for differential settlement of jet-grouted raft
ζ_{mr} = Coefficient for maximum bending moment of jet-grouted raft
ϕ' = Angle of internal friction of soil
ψ = Dilatancy angle of soil

References

Abaqus (2012). *Abaqus*, version 6.12, Dassault Systèmes, USA.

AGI (2012). Jet Grouting Guidelines, Associazione Geotecnica Italiana, Italy.

Algin, H. M. (2016). "Optimised design of jet-grouted raft using response surface method." *Comput Geotech*, Vol. 74, No. 4, pp. 56-73, DOI: 10.1016/j.compgeo.2015.12.012.

Arroyo, M., Gens, A., Alonso, E., Modoni, G., and Croce, P. (2007). *Informes sobre tratamientos de jet-grouting, ADIF LAV Madrid-Barcelona-Francia, Tramo Torrasa-Sants*, Rep. of the Univ. Politècnicha de Catalunya, Catalunya, Spain.

Bell, A. L. (1993). *Jet grouting*, Ground Improvement, M. P. Moseley, ed., Blackie, Boca Raton, Florida, 149-174.

Botto, G. (1985). "Developments in the techniques of jet grouting." *Proc., 12th Ciclo di Conferenze di Geotecnica*, Trevi, Vol. 1, pp. 81-90.

BS-EN-1994-1 (2004). *Eurocode 7-Geotechnical design*, European Committee for Standardization, Brussels, Belgium.

BS-EN-12716 (2001). *Execution of special geotechnical works: Jet grouting*, European Committee for Standardization, Brussels, Belgium, 38p.

Bustamante, M. (2002). *Les colonnes de jet grouting*, Report of the Seminar: Pathologies des Sols et des Foundations, France.

Bzówka, J. (2009). *Współpraca kolumn wykonywanych technika, iniekcji strumieniowej z podło_zem gruntowym (Interaction of jet grouting columns with subsoil)*, Silesian University of Technology, Gliwice, Poland.

Bzówka, J. and Pieczyrak, J. (2008). "Pull out and load tests for jet grouting columns." *Proc., Proc., XI Baltic Sea Geotechnical Conf., Polish Committee on Geotechnics and Gdansk Univ. of Technology*, Vol. 1, pp. 929-933.

Chu, E. H. (2005). *Turbulent Fluid Jet Excavation in Cohesive Soil, With Particular Application to Jet Grouting*, PhD, Massachusetts Institute of Technology, Cambridge, MA.

Cicognani, M. and Garassino, A. L. (1989). "Controlli nell'esecuzione dei trattamenti con jet grouting." *Proc., Proceedings of the 17th National Geotechnical Conference 1*, Associazione Geotecnica Italian, Vol. 1, pp. 97-105.

Croce, P. and Flora, A. (1998). "Effects of jet grouting in pyroclastic soils." *Rivista Italiana di Geotecnica* Vol. 29, No. 2, pp. 5-14.

Croce, P., Flora, A., and Modoni, G. (2001). "Experimental investigation of jet grouting." *Proc., Proceedins International Symposium 2001 A Geo-Odyssey*, Virginia Technical University, Vol. 1, pp. 245-259.

Croce, P., Flora, A., and Modoni, G. (2014). Jet Grouting: Technology, Design and Control, Taylor & Francis, Boca Raton, Florida.

Croce, P., Gajo, A., Mongiovì, L., and Zaninetti, A. (1994). "Una verifica sperimentale degli effetti della gettiniezione." *Riv. Ital. Geotec.*, Vol. 28, No. 2, pp. 91-101.

Croce, P. and Modoni, G. (2002). "Numerical modelling of jet-grouted foundations." *Proc., Proc., 5th European Conf. on Numerical Methods Geotechnical Engineering*, European Regional Technical Committee (ERTC7), Vol. 1, pp. 453-458.

Davis, E. H. and Taylor, H. (1962). "The movement of bridge approaches and abutments on soft foundation soils." *Civil Engineering Laboratories, University of Sydney*, Sydney, Australia.

DIN-4093 (2012). *Design of ground improvement: Jet grouting, deep mixing, or grouting*, Standard of the Deutsches Institut für Normung, Dusseldorf, Germany, 17p.

Falcao, J., Pinto, A., and Pinto, F. (2001). "Case histories and work performance of vertical jet grouting solutions." *Proc., Proceedings of the 4th International Conference on Ground Improvement*, Finnish Geotechnical Society, Vol. 1, pp. 165-171.

Flora, A. and Lirer, S. (2011). "Interventi di consolidamento dei terreni, tecnologie e scelte di progetto." *Proc., Proceedings of the 24th National Conference of Geotechnical Engineering* Innovazione tecnologica nell'Ingegneria Geotecnica', Vol. 1, pp. 87-148.

Flora, A., Modoni, G., Lirer, S., and Croce, P. (2013). "The diameter of single, double and triple fluid jet grouting columns: Prediction method and field trial results." *Geotechnique*,Vol. 63, No. 11, pp. 934-945, DOI: 10.1680/geot.12.P.062.

Garassino, A. L. (1997). *Design Procedures for Jet Grouting*, Seminar organised by THL Foundation Equipment Pte., Ltd., Singapore.

GI-ASCE (2009). *Jet Grouting Guideline*, Geo Institute of ASCE-Grouting Committee-Jet Grouting Task Force, USA.

Güneyisi, E., Gesoğlu, M., Algın, Z., and Mermerdaş, K. (2014). "Optimization of concrete mixture with hybrid blends of metakaolin and fly ash using response surface method." *Composites Part B: Engineering*, Vol. 60, No. 5, pp. 707-715, DOI: 10.1016/j.compositesb.2014.01.017.

Heng, J. (2008). *Physical modelling of jet grouting process*, PhD, University of Cambridge, Cambridge, UK.

Horikoshi, K. and Randolph, M. F. (1998). "A contribution to optimum design of piled rafts." *Geotechnique*,Vol. 48, No. 3, pp. 301-317, DOI: 10.1680/geot.1998.48.3.301.

Jaky, J. (1944). "The coefficient of earth pressure at rest." *Journal of the*

Society of Hungarian Architects and Engineers,Vol. 78, No. 22, pp. 355-358.

JJGA (2005). *Jet Grouting Technology: JSG Method, Column Jet Grouting Method*, Technical Information of the Japanese Jet Grouting Association, Japan, 80p.

Kutzner, C. (1996). *Grouting of rock and soil, A.A. Balkema*, Rotterdam, Netherlands.

Lesnik, M. (2001). "Methods to determine the dimension of jet-grouted bodies." *Proc., Proceedings of the 14th Young Geotechnical Engineers Conference*, Vol. 1, pp. 363-371.

Leung, Y. F., Klar, A., and Soga, K. (2010). "Theoretical study on pile length optimization of pile groups and piled rafts." *J Geotech Geoenviron*, Vol. 136, No. 2, pp. 319-330, DOI: 10.1061/(Asce) Gt.1943-5606.0000206.

Liang, F. Y., Chen, L. Z., and Shi, X. G. (2003). "Numerical analysis of composite piled raft with cushion subjected to vertical load." *Comput Geotech*,Vol. 30, No. 6, pp. 443-453, DOI: 10.1016/S0266-352x(03)00057-0.

Maertens, J. and Maekelberg, W. (2001). "Special applications of the jet grouting technique for underpinning works." *Proc., Proceedings of the 15th ICSMFE*, Vol. 1, pp. 1795-1798.

Miki, G. and Nakanishi, W. (1984). "Technical progress of the jet grouting method and its newest type." *Proc., Proceedings of the International Conference on In Situ Soil and Rock Reinforcement*, Vol. 1, pp. 195-200.

Modoni, G. and Bzowka, J. (2012). "Analysis of foundations reinforced with jet grouting." *J. Geotech Geoenviron*, Vol. 138, No. 12, pp. 1442-1454, DOI: 10.1061/(Asce)Gt.1943-5606.0000718.

Modoni, G., Croce, P., and Mongiovi, L. (2006). "Theoretical modelling of jet grouting." *Geotechnique*,Vol. 56, No. 5, pp. 335-347, DOI: 10.1680/geot.2006.56.5.335.

Myers, R. H., Montgomery, D. C., and Anderson-Cook, C. M. (2009). *Response surface methodology: Process and product optimization using designed experiments,* Wiley.

Nakanishi, K. and Takewaki, I. (2013). "Optimum pile arrangement in piled raft foundation by using simplified settlement analysis and adaptive step-length algorithm." *Geomech Eng*,Vol. 5, No. 6, pp. 519-540, DOI: 10.12989/gae.2013.5.6.519.

Pradeep, G. (2008). *Response surface method*, VDM Verlag Publishing, Saarbrücken, Germany.

Reul, O. and Randolph, M. F. (2004). "Design strategies for piled rafts subjected to nonuniform vertical loading." *J Geotech Geoenviron*, Vol. 130, No. 1, pp. 1-13, DOI: 10.1061/(Asce)1090-0241(2004) 130:1(1).

Schanz, T. (1998). *Zur modellierung des mechanischen verhaltens von reibungmaterialen,* PhD, Universität Stuttgart, Stuttgart, Germany.

Shahu, J. T. (2006). "Non-uniform granular pile–mat foundations: Analysis and model tests." *Geotech Geol Eng*,Vol. 24, No. 4, pp. 1065-1087, DOI: 10.1007/s10706-005-6316-z.

Tornaghi, R. and Pettinaroli, A. (2004). "Design and control criteria of jet grouting treatments." *Proc., Proceedings of the International Symposium on Ground Improvement*, Ecole Nationale des Ponts et Chaussees, Vol. 1, pp. 295-319.

Wang, Z.-F., Shen, S.-L., and Yang, J. (2012). "Estimation of the diameter of jet-grouted column based on turbulent kinematic flow theory." *Proc., Proceedings of the Conference on Grouting and Deep Mixing 2*, ASCE Geotechnical Special Publication, Vol. 1, pp. 2044-2051.

Whitcomb, P. J. and Anderson, M. J. (2004). *RSM simplified: Optimizing processes using response surface methods for design of experiments*, Taylor & Francis, New York.

Wright, S. J. and Reese, L. C. (1977). "Drilled shaft design and construction guidelines manual: Construction of drilled shafts and design for axial loading." U.S. Department of Transportation, Washington, DC, USA.

Xanthakos, P. P., Abramson, L. W., and Bruce, D. A. (1994). *Ground control and improvement*, John Wiley & Sons, New York.

Yahiro, T. and Yoshida, H. (1973). "Induction grouting method utilizing high speed water jet." *Proc., Proc., VIII Int. Conf. Soil Mechanics and Foundation Engineering*, USSR National Society, Vol. 1, pp. 402-404.